ORIGINAL ARTICLE

JBMR

Degree of Biological Apatite *c*-Axis Orientation Rather Than Bone Mineral Density Controls Mechanical Function in Bone Regenerated Using Recombinant Bone Morphogenetic Protein-2

Takuya Ishimoto,[1] Takayoshi Nakano,[1] Yukichi Umakoshi,[1] Masaya Yamamoto,[2] and Yasuhiko Tabata[2]

[1]Division of Materials and Manufacturing Science, Graduate School of Engineering, Osaka University, Osaka, Japan
[2]Institute for Frontier Medical Sciences, Kyoto University, Kyoto, Japan

ABSTRACT

The aim of the present study was to assess the bone regeneration process in defects introduced into rabbit long bones, which were regenerated with controlled release of recombinant bone morphogenetic protein-2 (rBMP-2). The orientation of the biological apatite (BAp) *c*-axis and bone mineral density (BMD) were compared as predictors of bone mechanical function. A 20-mm-long defect was introduced in rabbit ulnas, and 17 μg of rBMP-2 was controlled-released into the defect using a biodegradable gelatin hydrogel as the carrier. In the bone regeneration process, two characteristic phases may have been governed by different factors. First, new bone formation actively occurred, filling the bone defect with newly formed bone tissue and increasing the BMD. This process was regulated by the strong osteoinductive capacity of rBMP-2. Second, after filling of the defect and moderate BMD restoration, preferential BAp *c*-axis orientation began to increase, coincident with initiation of remodeling. In addition, the BAp *c*-axis orientation, rather than BMD, was strongly correlated with Young's modulus, an important index of bone mechanical function, particularly in the later stage of bone regeneration. Thus, preferential BAp *c*-axis orientation is a strong determinant and predictor of the mechanical function of tissue-engineered bone. Therefore, analysis of BAp preferential *c*-axis orientation in addition to measurement of BMD is crucial in assessment of bone mechanical function.

KEY WORDS: BIOLOGICAL APATITE (BAp); PREFERENTIAL ORIENTATION OF BAp *c*-AXIS; MICROBEAM X-RAY DIFFRACTION (μXRD); BONE REGENERATION; MECHANICAL FUNCTION

Introduction

In the field of bone-regenerative medicine, bone mechanical function is a frequent topic of discussion, reflecting the most important function of bone as the load-bearing structural element in animal bodies. It is generally accepted that the mechanical performance of bone can largely be attributed to the microarrangement of the inorganic and organic constituent phases of bone, biological apatite (BAp) crystals, and type I collagen fibers, respectively. To evaluate regenerated bone, however, soft X-ray photography, dual energy X-ray absorptiometry (DXA), and quantitative computed tomography (QCT) are generally used in clinical and experimental settings. These methods are able to evaluate bone mass and bone mineral density (BMD) but cannot assess bone microstructure, which may influence bone mechanical function. In previous studies, the limitations of these methods for evaluating the mechanical properties of regenerated bone have been noted.[1–3]

It is commonly recognized that crystallographic texture and orientation—orderly arrangements of elemental atoms, ions, and molecules—are strongly related to the function of materials, including metals, ceramics, polymers, etc. Bone BAp and collagen are known to have specific crystallographic textures, depending on the bone type.[4,5] BAp crystallizes on the collagen template in an epitaxial manner[6] through an in vivo self-assembly process. BAp has a hexagonal-based lattice that normally demonstrates greater anisotropy than materials with cubic-based lattices. Indeed, BAp shows anisotropy in intrinsic mechanical properties such as Young's modulus. Nanoindentation studies of hydroxyapatite single crystals[7,8] show that Young's modulus along the *c*-axis is greater than that along the *a*-axis; this is attributed to the anisotropic arrangement of its constituent ions.[9] Hence, the

Received in original form June 27, 2012; revised form October 16, 2012; accepted November 12, 2012. Accepted manuscript online November 26, 2012.
Address correspondence to: Takayoshi Nakano, PhD, Division of Materials and Manufacturing Science, Graduate School of Engineering, Osaka University, 2-1, Yamada-oka, Suita, Osaka 565-0871, Japan. E-mail: nakano@mat.eng.osaka-u.ac.jp

Journal of Bone and Mineral Research, Vol. 28, No. 5, May 2013, pp 1170–1179
DOI: 10.1002/jbmr.1825

degree of directionality of the BAp *c*-axis may be a determinant of bone mechanical function. Furthermore, BAp crystallinity, measured by Fourier transform infrared (FTIR) spectroscopy and Raman spectroscopy, has been associated with elastic modulus, fatigue properties, and fracture risk.[10,11] Crystallinity reflects the *c*-axis length of BAp and may be related to BAp texture.

The crystallographic texture of BAp has been analyzed through X-ray diffraction,[4,5,12,13] neutron diffraction,[14,15] synchrotron diffraction,[16] FTIR spectroscopy,[10,17] and Raman spectroscopy,[11,18] and collagen has been analyzed through X-ray diffraction,[12] polarized light microscopy,[19,20] and recently, Raman spectroscopy.[21] Based on these studies, it is becoming evident that in normal bone, BAp and/or collagen texture significantly contributes to the mechanical properties of bone. Sasaki and colleagues[22] reported that the angular dependence of Young's modulus from the longitudinal axis of the bovine femur was explained by the distribution of the BAp *c*-axis orientation. Martin and colleagues[23,24] demonstrated that collagen fiber orientation was an important determinant of the tensile and bending strength of bovine long bones. Hence, BAp and/or collagen orientation is a likely contributor to and predictor of mechanical function in normal bones.

However, recovery of bone crystallographic texture during bone regeneration and the contribution of bone crystallographic texture to the mechanical function of regenerated bone is less well understood. Previous reports have described the BAp and/or collagen orientation of regenerated bone[25–27]; however, these studies mapped the distribution of BAp particle orientation rather than the crystallographic orientation at only a few time points. To our knowledge, there is no information on recovery of crystallographic texture and its correlation with mechanical function. To evaluate these aspects, a combination of microbeam X-ray diffraction (μXRD) for analyzing the preferential orientation of the BAp *c*-axis[28–30] and nanoindentation mechanical testing[31] is a powerful approach. Both of these approaches can be applied to regenerated bone samples with small size and irregular shape, as a sample 500 μm in diameter is sufficient for both analyses. Nakano and colleagues[28] demonstrated the potential of μXRD for quantitatively analyzing the preferential BAp *c*-axis orientation in regenerated bone. Moreover, nanoindentation testing conditions have been optimized for immature regenerated bone,[31] which shows highly viscoelastic deformation behavior.

In the present study, controlled release of recombinant bone morphogenetic protein-2 (rBMP-2), a well-established and potent tissue engineering technique for rapid bone reconstruction,[32,33] was used for bone regeneration. The bone regeneration process was quantitatively analyzed by evaluating the recovery in preferential BAp *c*-axis orientation. The BAp *c*-axis is parallel to the collagen fiber direction in bone[34]; therefore, the BAp *c*-axis orientation can be used to determine the collagen orientation. The recovery of BMD was also evaluated during bone regeneration and compared with that of BAp orientation. Finally, correlations between the BAp *c*-axis orientation, BMD, and Young's modulus as an important index of bone mechanical function were explored quantitatively and statistically to evaluate BAp *c*-axis orientation as a potential determinant and predictor of mechanical function in tissue-engineered bone.

Materials and Methods

Animals and surgical procedures

Eighteen skeletally mature New Zealand white rabbits (male, ~3 kg; Shimizu Laboratory Supply, Kyoto, Japan) were used in this study. The animals were housed individually, provided commercial food and water *ad libitum*, and kept under controlled light conditions (12/12 hour light/dark cycle) throughout the experiment.

After 1 week of acclimation, a segmental defect was introduced at the mid-diaphysis of both ulnas using surgical procedures described.[35] A 4-cm-long incision was made in both forelimbs to expose the ulnas and 20-mm-long critical-sized segmental defects were created in the ulnar mid-diaphyses with a surgical oscillating saw supplemented by copious sterile saline water irrigation under anesthesia. Gelatin hydrogel incorporating 17 μg of rBMP-2 was applied to the defect in the left ulna for controlled release of rBMP-2, while no treatment was applied to the right ulna (control). The hydrogel water content governs the in vivo release profile of rBMP-2 by controlling the rate of hydrogel degradation. A hydrogel with 97.8 wt% water content was used in this study. Preparation of the gelatin hydrogel incorporating rBMP-2 has previously been described in detail; 17 μg of rBMP-2 was confirmed to be sufficient for osteoinduction for a 20-mm rabbit ulnar defect.[36] Internal fixation of osteotomized ulnas was not necessary because of the fibro-osseous union between the residual ulnae and neighboring radii. Soft tissue was approximated with interrupted 4–0 Vicryl (Ethicon Inc., Somerville, NJ, USA) and the skin was closed with 3–0 silk sutures.

Rabbits were randomly assigned to five groups based on healing periods. The animals were allowed to freely perform weight-bearing activities in the cage after the operation and were sacrificed by an intravenously administered overdose of sodium pentobarbital at 2, 4, 6, 12, or 24 weeks after the operation. Rabbits were also prepared as an intact baseline; they were euthanized after acclimation without being osteotomized.

All of the animal experiments were approved by the Kyoto University Committee for Animal Experimentation.

Sample preparation

The ulnas and the neighboring radii of both forelimbs were removed together and immersed in 10 wt% formalin neutral buffer solution for 2 weeks to avoid degradation of the organic matrix. The regenerated portion and adjacent normal portion were carefully cut perpendicular to the long bone axis using a circular saw (Model 660; South Bay Technology Inc., San Clemente, CA, USA) with a diamond wheel 0.30 mm thick and 100 mm in diameter. Sample cross-sections were polished to obtain a smooth surface for μXRD analysis and nanoindentation testing. After grinding with silicon carbide paper of progressively finer grit (600, 800, and 1200) under deionized water, the specimen surfaces were then polished with a microcloth (TEXMET; Buehler Ltd, Lake Bluff, IL, USA) with a 0.05-μm alumina suspension. Specimen surfaces were finished with a plane microcloth. The samples were then ultrasonically cleaned in deionized water for 5 minutes to remove surface debris before

drying in air. The water temperature was held below 37°C during ultrasonic exposure to prevent alterations in the mechanical properties of the bone specimens.

Radiography

Soft X-ray photographs were taken at 2, 4, 6, 12, and 24 weeks postoperatively after the removal of the ulnas and radii using an X'sy (Shimadzu Co., Kyoto, Japan), at 40 kV, 80 mA, and 71 msec radiation.

Density-based analysis by peripheral QCT

BMD was measured in the removed ulnas with the neighboring radii in formalin using an XCT Research SA+ system (Stratec Medizintechnik GmbH, Birkenfeld, Germany) at 50.7 kV and 0.276 mA with a resolution of $80 \times 80 \times 460$ μm. The BMD measurements were performed at four points along the 20-mm-long regenerated portion at intervals of 4 mm, and at corresponding sites on the intact baseline samples, determined by projection images (scout view).

The data for each voxel were exported in ASCII format (CSV file) into Microsoft Excel software. The cross-sectional area and average BMD for each regenerated ulna were calculated using Microsoft Excel software based on the BMD values for the individual voxels. Regenerated bone tissue was judged above a threshold value of 267 mg/cm^3;[31] no distinction between cortical and cancellous bone was made in this study. BMD was then analyzed in the same local region of about 500×500 μm for the cross-section (local BMD) at which the μXRD analysis was performed.

Analysis of preferential BAp *c*-axis orientation by microbeam X-ray diffraction

X-ray diffraction analysis was carried out using a μXRD system (M18XHF22-SR; Mac Science Co., Yokohama, Japan). Cu-Kα radiation with a wavelength of 0.154 nm generated at a tube voltage of 90 kV and a tube current of 40 mA was used. The incident beam was collimated into a circular spot of 100 μm in diameter by a metal collimator. The scattered radiation was detected by a curved position-sensitive proportional X-ray counter (PSPC) with its spatial dimension along the 2θ axis and an angular resolution <0.15 degrees. Using this 1D PSPC, multiple peaks could be detected simultaneously. Therefore, the specimen could be swung and rotated over an appropriate range to obtain homogeneous diffraction data for peaks used for analysis of BAp *c*-axis preferential orientation.

The two representative diffraction peaks for BAp, (002) and (310) appearing at Bragg angles (2θ) of 25.9 degrees and 39.8 degrees, respectively, were detected for BAp *c*-axis orientation analysis. Hence, specimen swing and rotation were determined in Euler angles as follows: 11.8 degrees $\leq \omega \leq 22.8$ degrees; -0.6 degrees $\leq \chi \leq 0.6$ degrees; and 0 degrees $\leq \varphi \leq 180$ degrees. Thus, XRD peaks were obtained from an irradiated area of ~500 μm in diameter on the specimen surface. Details of conditions for μXRD analysis have been described previously.[4]

The degree of orientation of the *c*-axis in the BAp crystallites was determined as the relative intensity ratio of the (002) diffraction peak to the (310) peak in the X-ray profile. Because the (002) plane is a typical plane representing the *c*-axis and the (310) plane is a perpendicular plane to the (002) plane in a hexagonal lattice, the intensity ratio of (002)/(310) is appropriate for evaluating the preferential orientation of the BAp *c*-axis. The intensity ratio increases with an increase in the degree of preferential orientation of the *c*-axis of BAp. Randomly oriented apatite (hydroxyapatite) powders fabricated by a wet process have been reported to have a relative intensity ratio of 2.[4]

In long bones, the BAp *c*-axis is preferentially oriented along the longitudinal axis aligned with the collagen matrix.[12,29] In this study, therefore, the μXRD measurements were performed on the ulnar transverse cross-sections with a reflection optical system, resulting in orientation data along the longitudinal axis of the bone. Because of the specimen swing and rotation described above, diffraction of (002) and (310) could be detected within an angular range of about 10 degrees from the normal direction of the cross-section. The measurements were performed for 1000 seconds on the ulnar cross-section near the neighboring radius.

Biomechanical assessment by nanoindentation

After the samples were dried, Young's modulus was measured along the ulnar longitudinal direction using a nanoindentation system (ENT-1100a; Elionix Ltd., Tokyo, Japan) with a Berkovich diamond indenter at 25°C. Five indentations were created on each polished specimen surface in the 500-μm-diameter region in which the μXRD analysis and local BMD measurements were performed, and the results were averaged. Load–depth measurements were carried out on the specimen surface according to established methods.[31] Briefly, the loading/unloading rate and maximum load were 400 μN/s and 6000 μN, respectively. To minimize the effects of the viscoelastic behavior of bone, a constant maximum load was held for 180 seconds before unloading, as determined previously.[31] All measurements also included a second constant load held for 30 seconds at 10% of the maximum load to establish the thermal drift rate and correct the data. Young's modulus was determined by the method of Oliver and Pharr.[37] The Poisson ratio of bone was assumed to be 0.3 and the region between 95% and 50% of the maximum load was used to calculate the slope of the unloading curve.

To assess the effect of the 2-week formalin fixation on Young's modulus, the nanoindentation test was performed on the rabbit ulnar cortical bone along the long axis of the bone before and after formalin fixation, under the same testing conditions. Young's moduli before and after formalin fixation were significantly and linearly correlated over a relatively wide range. The regression formula was (Young's modulus after formalin fixation) = 0.994 (Young's modulus before formalin fixation), and the coefficient of determination (R^2) and p value were 0.93 and <0.05, respectively. Thus, no effect of the 2-week formalin fixation on Young's modulus was observed.

Statistical analysis

All data are presented as means ± standard deviations (SDs). Statistical comparisons between two means were performed using a two-tailed unpaired Student's *t* test. Pearson's

correlations and multiple linear regression analyses were used to determine significant determinants for Young's modulus. In the multiple linear regression analysis, BMD and BAp *c*-axis orientation were considered independent variables. The multiple regression coefficient (β) was used to identify the dominant determinant. A value of $p < 0.05$ was considered statistically significant. SPSS version 14.0J software (SPSS Japan Inc., Tokyo, Japan) for Microsoft Windows was used for all statistical analyses.

Results

Effect of controlled release of rBMP-2 on bone regeneration of the segmental ulnar defect

Soft X-ray photographs were taken of the removed ulnas and neighboring radii at 2, 4, 6, 12, and 24 weeks after osteotomy (Fig. 1). Throughout the experimental period of 24 weeks, there was little new bone formation or radiolucent nonunion in the 20-mm-long defects without rBMP-2 treatment (Fig. 1*F–J*). In contrast, with controlled release of rBMP-2, radiopacity was observed in the defect and the defect was filled with bony tissues within 4 weeks of the operation (Fig. 1*A–E*). The interface between the regenerated and host bone became less evident as regeneration progressed, and cortical bone-like structure was obvious after 12 weeks. A marked effect of rBMP-2 on bone regeneration was clearly observable in the soft X-ray photographs as an increased mass of bone tissue newly formed in the ulnar defect.

Table 1 shows the cross-sectional area of the regenerated ulnae with and without rBMP-2. The group with rBMP-2 release had much larger cross-sections than the control group at each time point over 4 weeks. The critically sized 20-mm-long defect could not be spontaneously regenerated, as demonstrated by the substantially smaller cross-sectional area of the control samples compared to the intact baseline. These results clearly demonstrate that controlled release of rBMP-2 from a degradable gelatin hydrogel markedly enhanced new bone formation in 20-mm segmental defects in rabbit ulnas. The cross-sectional area in the rBMP-2 group was largest at 4 weeks, then decreased gradually to the intact level.

BMD histograms at all regeneration time points are shown for the rBMP-2 group in Fig. 2. The BMD peak appeared at 4 weeks and gradually shifted to higher BMD values. The BMD distribution became quite similar to the intact baseline at 24 weeks. A higher frequency of low BMD was present at 6 weeks (Fig. 2*C*, arrow). This characteristic distribution of BMD may be related to formation of the marrow cavity, which is clearly observable in the pQCT reconstructed images (insets, Fig. 2*B*, *C*). The lower BMD distribution at 6 weeks indicates bone tissue being absorbed to form a marrow cavity. An osteon-like structure

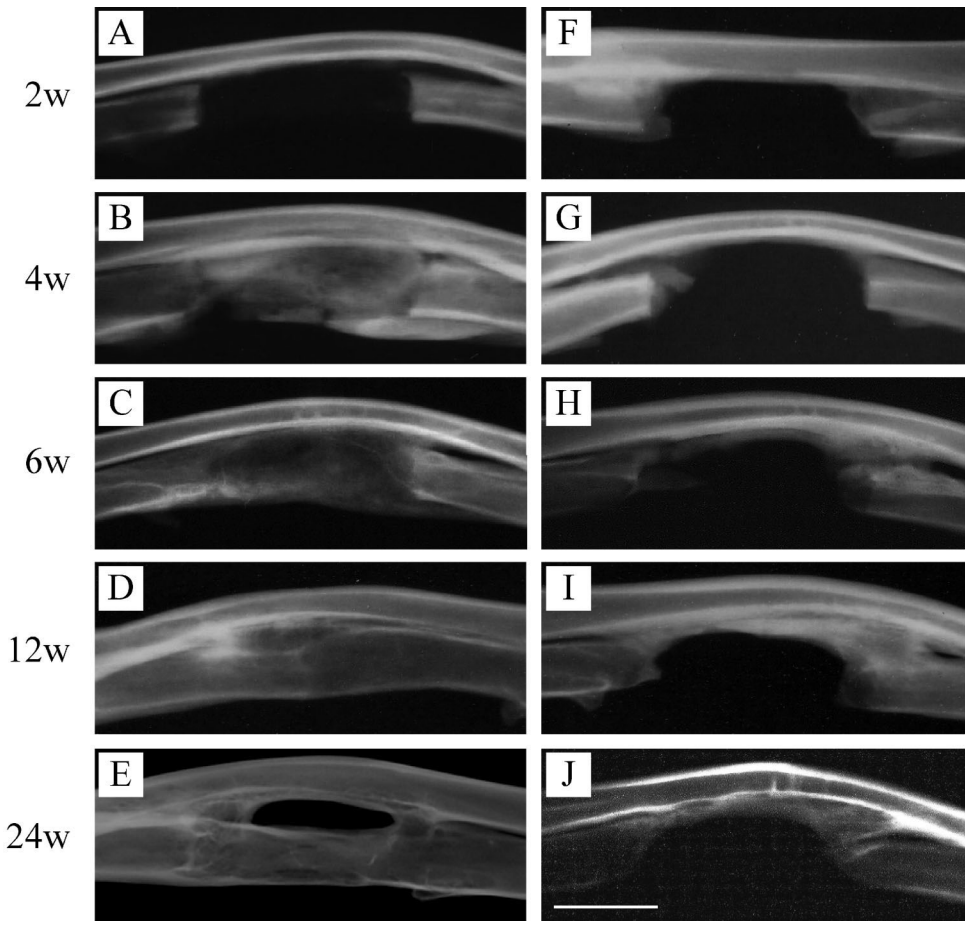

Fig. 1. Soft X-ray photographs of rabbit ulna defects regenerated for 2 (*A*, *F*), 4 (*B*, *G*), 6 (*C*, *H*), 12 (*D*, *I*), and 24 (*E*, *J*) weeks, with (*A–E*) and without (*F–J*) controlled release of rBMP-2. Scale bar, 10 mm.

Table 1. Cross-Sectional Area of Regenerated Bone at the Ulnar Defect With and Without Controlled Release of rBMP-2

	rBMP-2 (mm)	Control (mm)
2 weeks	3.40 ± 4.10	1.86 ± 2.24[a]
4 weeks	19.64 ± 12.66[b]	5.33 ± 6.93
6 weeks	14.05 ± 4.85[b]	2.17 ± 0.27[a]
12 weeks	13.36 ± 4.40[b]	2.76 ± 0.39[a]
24 weeks	9.54 ± 1.34[b]	4.49 ± 0.68[a]
Intact	9.96 ± 0.39	

Values are mean $\pm$ SD.
rBMP-2 = recombinant bone morphogenetic protein-2.
[a,b]Significant differences from the intact baseline and control, respectively, at $p < 0.05$.

was observed in the regenerated bone at 6 weeks (data not shown), possibly indicating the presence of remodeling activity. The remodeling process is essential for establishment and improvement of bone microstructure, including BAp crystallographic texture.

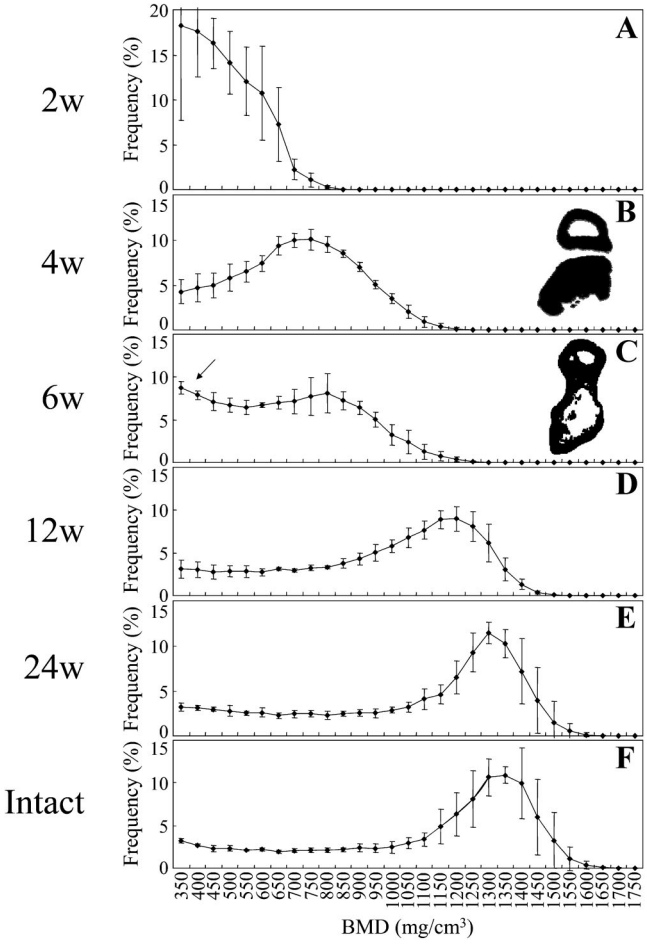

Fig. 2. BMD distribution of the regenerated bone at 2 (*A*), 4 (*B*), 6 (*C*), 12 (*D*), and 24 (*E*) weeks postoperatively, and for intact bone (*F*). The insets in *B* and *C* are typical cross-sections of the regenerated bone.

Analysis of preferential BAp *c*-axis orientation

The appearance and degree of BAp *c*-axis orientation in the regenerated and adjacent normal bone are shown at 6 weeks in Fig. 3. A larger intensity ratio indicates a higher degree of BAp *c*-axis orientation in the longitudinal direction. Preferential BAp *c*-axis orientation in the regenerated bone tissues was significantly lower than that in normal bone ($p < 0.05$), although the ulnar defect appeared to be completely filled with newly formed bone.

Recoveries of BAp *c*-axis orientation and local BMD are summarized in Fig. 4. Both measurements were performed in the same local area $\sim$500 μm in diameter. During the early phase of regeneration (2–4 weeks postoperatively), the diffracted intensity ratio of (002)/(310) in the regenerated bone tissue was much lower than that in the non-defected portion. Significant increases were observed from 2 to 4 weeks, 6 to 12 weeks, and 12 to 24 weeks in local BMD, and from 4 to 6 weeks and 12 to 24 weeks in the intensity ratio. There were no significant differences from baseline (intact bone) at 24 weeks in either local BMD or the intensity ratio. Thus, in regeneration of rabbit ulnas with controlled release of rBMP-2, recovery of the preferential BAp *c*-axis orientation tends to follow that of BMD.

Biomechanical evaluation by nanoindentation

As an index of bone mechanical function, Young's modulus was measured by the nanoindentation technique in the regenerated and intact bone samples. Because there was little new bone formation, nanoindentation measurements could not be performed at 2 weeks. Due to the recoveries in BMD and preferential BAp *c*-axis orientation, Young's modulus increased monotonically as a function of the regeneration period; the values for regenerated bones 4, 6, 12, and 24 weeks postoperatively and for intact bone were 12.1 ± 1.2 ($p < 0.05$ versus intact bone), 17.0 ± 0.9 ($p < 0.05$ versus intact bone), 19.9 ± 2.5

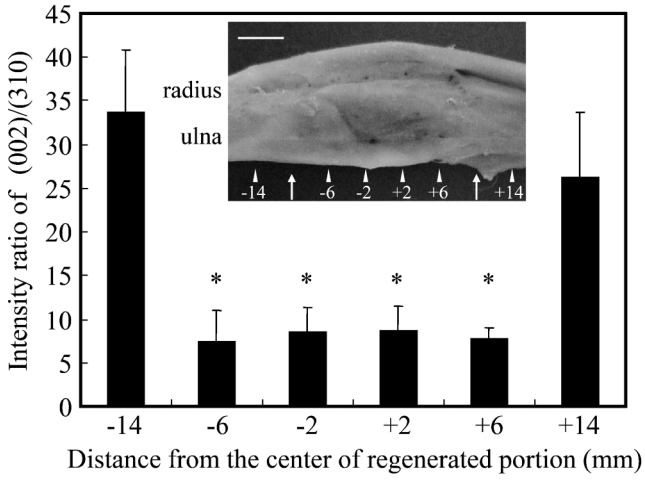

Fig. 3. Appearance of the regenerated bone and typical example of the degree of BAp *c*-axis orientation in regenerated and adjacent normal bone at 6 weeks. Arrows indicate the edge of the defect. Scale bar, 5 mm. *$p < 0.05$, significant versus both proximal (−14) and distal (+14) intact portions of the residual ulna.

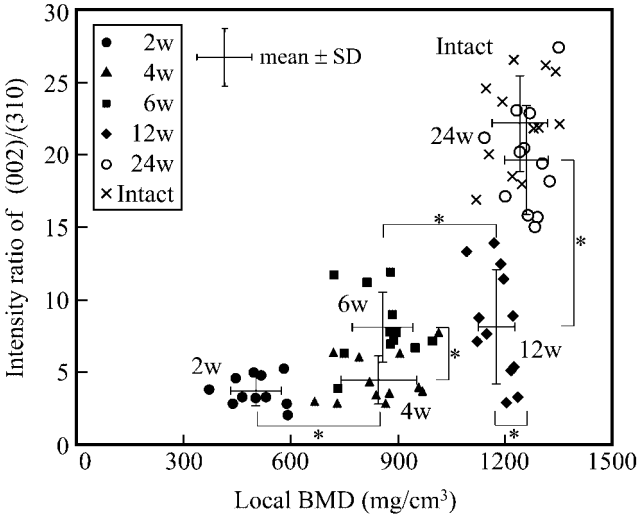

Fig. 4. Recovery of local BMD and BAp *c*-axis alignment in the regenerated ulna. $^{*}p < 0.05$, significant difference. Results were not significant versus the intact baseline at 24 weeks for both local BMD and BAp *c*-axis orientation.

($p < 0.05$ versus intact bone), 26.1 ± 1.5 ($p < 0.05$ versus intact bone), and 31.5 ± 0.4, respectively. Twelve weeks postoperatively, the regenerated bone tissue had a much lower Young's modulus than the intact baseline despite high restoration of BMD.

Contributions of BMD and BAp *c*-axis orientation to Young's modulus

Figure 5 shows correlations between Young's modulus and local BMD or BAp *c*-axis orientation at each time point. A significant correlation is represented by a straight line. Young's modulus was significantly correlated with BMD only at 4 weeks ($R^2 = 0.73$, $p < 0.05$). In contrast, at 6, 12, and 24 weeks postoperatively, Young's modulus was significantly correlated with the intensity ratio of (002)/(310) ($R^2 = 0.62$, $p < 0.05$ at 6 weeks; $R^2 = 0.68$, $p < 0.05$ at 12 weeks; and $R^2 = 0.59$, $p < 0.05$ at 24 weeks).

Based on the multiple linear regression analysis, Young's modulus can be expressed as a function of BMD and BAp *c*-axis orientation as follows:

$$\text{Young's modulus} = 7.3 + 3.5\text{x}10^{-6}(\text{BMD}) + 0.74(\text{BAp } c\text{-axis orientation}) \quad (1)$$

The adjusted R^2 for this regression was 0.83, indicating that Young's modulus is largely explained using BMD and BAp *c*-axis orientation as explanatory variables. The multiple regression coefficients (β) and *p* values for BMD and BAp *c*-axis orientation were (0.26, <0.05) and (0.73, <0.05), respectively. Thus, BAp *c*-axis orientation was determined to be the dominant contributing factor to the Young's modulus of the regenerated bone.

Discussion

In the present study, regeneration of rabbit ulnar defects with controlled release of rBMP-2 from degradable gelatin hydrogel was evaluated using BMD, degree of preferential BAp *c*-axis orientation, and Young's modulus. The relative contributions of BMD and preferential BAp *c*-axis orientation to Young's modulus were also analyzed. The recovery of long bones with controlled release of rBMP-2 was observed to have two main phases, BMD restoration and subsequent reconstruction of the BAp *c*-axis orientation. The two phases appear to be governed by different factors.

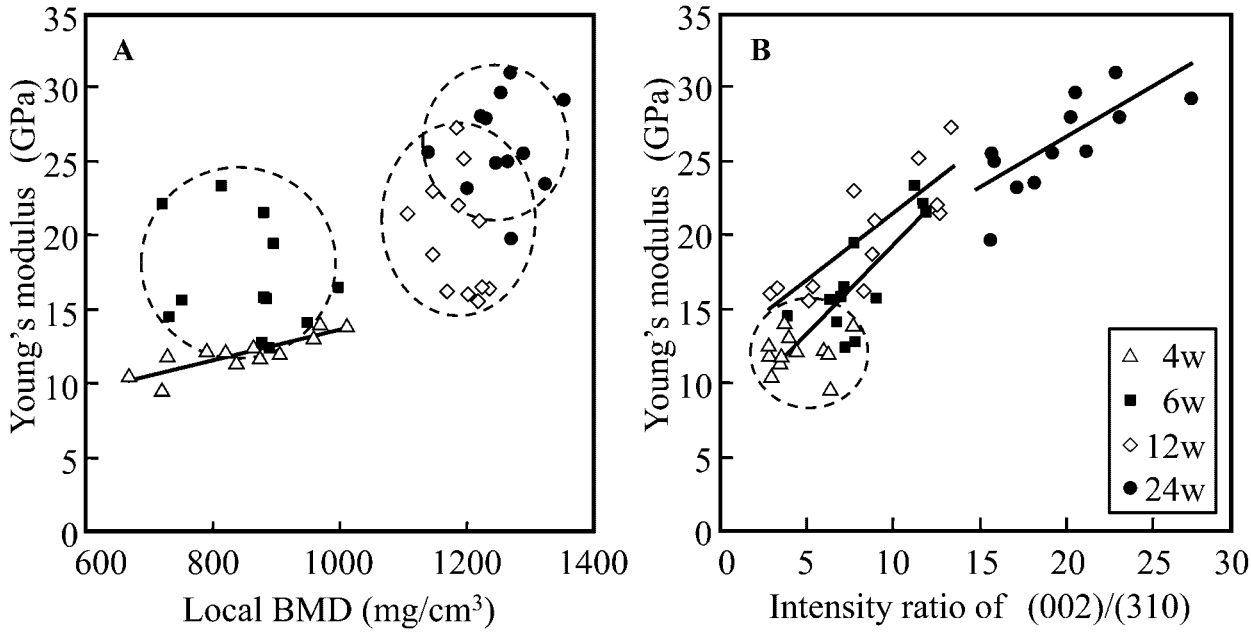

Fig. 5. Correlations between Young's modulus and local BMD (*A*) and BAp *c*-axis orientation (*B*) at 4, 6, 12, and 24 weeks. Straight lines represent significant correlations between the parameters.

In the early phase of bone regeneration, the segmental defect was filled with bone tissue due to rapid new bone formation. During this phase, the regenerated bone was less mineralized and had very little BAp *c*-axis orientation along the longitudinal axis of the rabbit ulna. This suggests that the early regenerated bone has a poorly organized microstructure and the BAp *c*-axis orientation is nearly random. BMD continued to increase while the degree of BAp *c*-axis orientation remained low. New bone formation in the defect and mineralization were clearly accelerated by the strong osteoinductive capacity of rBMP-2, and the defect was completely filled with new bone 4 weeks after the operation. The bone regeneration rate induced by rBMP-2 was most rapid 2 to 4 weeks after the osteotomy (Fig. 1). Hence, bone regeneration peaked ~2 weeks after the point at which most of the rBMP-2 had been released, as the half-life for controlled release of rBMP-2 from the hydrogel was <1 week under these conditions.[38] rBMP-2 induces differentiation of pluripotent cells into bone-forming cells,[39,40] converts non-osteogenic differentiation pathways into osteoblastic lineages,[41,42] and stimulates osteoblastic maturation,[41] which results in stimulated bone formation. Our results are consistent with an in vivo study in which ectopic bone formation in mice occurred 2 weeks after implantation of human bone marrow–derived stromal cells and rBMP-2.[43]

rBMP-2-induced bone union may result in stress transmission to the ulna through the regenerated bone. In the present study, a significant increase in the degree of BAp *c*-axis orientation was observed subsequent to bone union and partial restoration of BMD, indicating that applied stress is related to an increase in the BAp *c*-axis orientation in the regenerated bone tissue. To confirm the above hypothesis, the relationship between the degree of recovery of preferential BAp *c*-axis orientation and applied stress on the regenerated portion was evaluated. Because of the difficulty in direct measurement of the applied stress, the stress along the longitudinal axis of the bone was roughly estimated to correlate with the Young's modulus in the same direction, based on the assumption that the strain on the regenerated portion is constant and governed by the neighboring radius. Data from 6, 12, and 24 weeks were used in this analysis because reestablishment of the bone microstructure through remodeling had begun by 6 weeks postoperatively, whereas remodeling was not evident at 4 weeks. A significant positive correlation ($R^2 = 0.76$, $p < 0.05$) between BAp *c*-axis orientation and the applied stress index was observed (Fig. 6). Thus, applied stress may play an important role in controlling BAp *c*-axis orientation along the stress axis in regenerated bone. In a previous report, the degree of recovery of preferential BAp *c*-axis orientation along the long bone axis was strongly correlated with the magnitude of locally applied stress in the same direction, using a spontaneous healing model with a 10-mm-long defect in rabbit ulnas.[30] In intact bone, applied stress also plays an important role in establishment and reestablishment of BAp *c*-axis orientation.[4,44] For example, in a dentulous mandible, the BAp *c*-axis generally aligns uniaxially with the mesiodistal direction in which the bending moment causes principal stress; the BAp *c*-axis orientation changes locally along the in vivo biting and chewing stress axis just beneath the tooth. It has been demonstrated that in reconstruction of bone microstructure

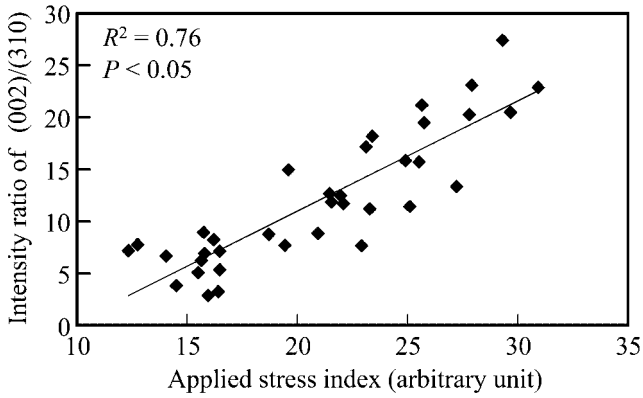

Fig. 6. Correlation between the degree of BAp *c*-axis orientation in the regenerated bone and the applied stress index. Data for 6, 12, and 24 weeks postoperation were used in this analysis.

such as BAp arrangement and recovery of bone mass, changes in macroscopic architecture and density depend on physiological in vivo stress conditions. In addition, reconstruction of bone tissue through remodeling is assumed to occur mainly through osteoclastic bone resorption and osteoblastic bone formation. Immature bone with little BAp *c*-axis orientation that initially forms in the defective site is replaced by mature and highly oriented bone through remodeling as bone regeneration proceeds. At the same time, BAp *c*-axis orientation develops in response to in vivo stress conditions. In the present study, the BMD distribution at 6 weeks (Fig. 2*C*) indicates that bone remodeling had begun; as a result, the marrow cavity was formed. Furthermore, an osteon-like structure was observed in the cross-section of the regenerated bone at 6 weeks. Preferential BAp *c*-axis orientation began to increase at the same time as remodeling was observed. It is poorly understood when and how remodeling begins during bone regeneration, although it is necessary for reconstruction of bone microstructure. rBMP-2 released from a gelatin hydrogel may regulate remodeling, because osteoclasts express rBMP-2 receptors and rBMP-2 directly stimulates osteoclast differentiation[45,46] and activation.[47] rBMP-2 also stimulates both bone formation and bone resorption.[48]

The amount and density of the mineral component (BAp) have conventionally been thought to be predictors of bone strength. For bone regeneration, most bone assessments have been conducted using bone mass and BMD. However, several reports have suggested the limitations of bone mass and BMD as sole predictors of the strength of regenerated bone tissue.[1–3] Watanabe and colleagues[2] reported an interesting experimental result using a rat femoral fracture model. Although increases in ash density and ash content were complete 8 weeks after surgery, tensile and torsional properties continued to improve. Thus, the mechanical properties of the bone improved without an increase in mass or density in the later phase of healing. A similar dissociation between mineral content and mechanical properties has also been reported for regenerated sheep tibias and rat fibulas.[1,3] These findings demonstrate that the mechanical properties of regenerated bone cannot be described simply by the content or density of BAp, especially in the later

phases of bone regeneration. These previous results are consistent with the results of this study, indicating that BMD can explain Young's modulus only in the early stage of bone healing (4 weeks), but not after 6 weeks. Liu and colleagues[25] postulated that impaired mechanical properties, despite nearly fully restored bone mineral content, may be at least partly due to BAp particle orientation; however, statistical evaluations were not conducted to test this hypothesis. The results of the present study clearly demonstrate that the BAp *c*-axis (and associated collagen) orientation is the dominant factor in determining the mechanical properties of the regenerated bone. Because of the intrinsic mechanical anisotropy of BAp and related collagen, their directional arrangement produces anisotropic bone mechanical function. This mechanical anisotropy increased as the BAp orientation became prominent. Therefore, Young's modulus parallel to the BAp *c*-axis orientation direction increased without a significant increase in BAp density.

Analysis of bone quality is essential for appropriate assessment of bone microstructure and corresponding mechanical function. Recent FTIR and Raman spectroscopy studies have contributed to an understanding of bone mechanical function, providing indicators of the compositional and biochemical status of bone.[49] The BAp crystallinity index, which reflects mineral crystal size (*c*-axis length) and stoichiometric perfection, has been correlated with intrinsic material properties such as elasticity and fatigue properties[11] and risk of fractures.[10] Collagen maturity, defined as the ratio of pyridinoline (mature) and dihydroxylysinonorleucine (immature) cross-links, has been found to be predictive of the risk of fractures.[10]

Among the many candidate parameters of bone quality, including indices derived by FTIR or Raman spectroscopy,[10,11,17,18,49] microarchitecture of the trabecular bone,[50] microdamage accumulation,[51] degree of mineralization,[51] turnover cycle,[52] and advanced glycation end-product (AGEs) cross-links,[53] preferential orientation of the BAp *c*-axis is a promising parameter that dominates bone mechanical function. The present study demonstrates that even using advanced tissue-engineering techniques, it is difficult to achieve appropriate bone microstructure and mechanical function. Novel bone regenerative methods must direct recovery of the bone microstructure, including the BAp *c*-axis orientation, as well as BMD. These findings are also applicable to treatment of osteoporosis, because the BAp *c*-axis orientation is a useful index for evaluating diseased bone.[54,55]

The ultimate goal in the field of bone biomechanics is to identify indices predictive of fracture risk that reflect whole-bone properties. In the present study, local mechanical properties were assessed by nanoindentation, which has not yet been demonstrated to correlate with whole-bone properties. To validate the usefulness of the BAp *c*-axis orientation as a predictor of fracture risk, further studies are essential to clarify the correlation between local mechanical properties and fracture risk, including both local (eg, nanoindentation) and whole-bone (eg, three-point bending) mechanical testing. In addition, μXRD analysis with the reflective optical system used in the present study is invasive. Less or noninvasive analytical methods should be established for clinical evaluation of BAp *c*-axis orientation.

In conclusion, preferential orientation of the BAp *c*-axis was demonstrated to be a promising index for determining and predicting Young's modulus in regenerated or tissue-engineered bone tissue. BAp *c*-axis orientation recovers after BMD; therefore, Young's modulus in the regenerated bone remains significantly lower than that of intact bone even when the BMD has largely recovered. Establishment of BAp crystallographic texture in the regenerated bone appears to be affected by in vivo applied stress through bone remodeling activities involving absorption and reconstruction of bone tissue.

Disclosures

All authors state that they have no conflicts of interest.

Acknowledgments

This work was supported by the Funding Program for Next Generation World-Leading Researchers and Grants-in-Aid for Young Scientists (B) from the Japan Society for the Promotion of Science (JSPS).

Authors' roles: Study design: TN, YU, and YT. Study conduct: TI, TN, and MY. Data collection: TI and TN. Data analysis: TI and TN. Data interpretation: TI, TN, and YU. Drafting manuscript: TI and TN. Revising manuscript content: TI and TN. Approving final version of manuscript: All authors. TN takes responsibility for the integrity of the data analysis.

References

1. Manjubala I, Liu Y, Epari DR, Roschger P, Schell H, Fratzl P, Duda GN. Spatial and temporal variations of mechanical properties and mineral content of the external callus during bone healing. Bone. 2009;45:185–92.
2. Watanabe Y, Takai S, Arai Y, Yoshino N, Hirasawa Y. Prediction of mechanical properties of healing fractures using acoustic emission. J Orthop Res. 2001;19:548–53.
3. Chakkalakal DA, Strates BS, Mashoof AA, Garvin KL, Novak JR, Fritz ED, Mollner TJ, McGuire MH. Repair of segmental bone defects in the rat: an experimental model of human fracture healing. Bone. 1999;25:321–32.
4. Nakano T, Kaibara K, Tabata Y, Nagata N, Enomoto S, Marukawa E, Umakoshi Y. Unique alignment and texture of biological apatite crystallites in typical calcified tissues analyzed by microbeam X-ray diffractometer system. Bone. 2002;31:479–87.
5. Nightingale JP, Lewis D. Pole figures of the orientation of apatite in bones. Nature. 1971;232:334–5.
6. Landis WJ. The strength of a calcified tissue depends in part on the molecular structure and organization of its constituent mineral crystals in their organic matrix. Bone. 1995;16:533–44.
7. Zamiri A, Dea S. Mechanical properties of hydroxyapatite single crystals from nanoindentation data. J Mech Behav Biomed Mater. 2011;4:146–52.
8. Viswanath B, Raghavan R, Ramamurty U, Ravishankar N. Mechanical properties and anisotropy in hydroxyapatite single crystals. Scripta Mater. 2007;57:361–4.
9. Elliott JC. Structure and chemistry of the apatites and other calcium orthophosphates. Amsterdam: Elsevier; 1994.
10. Gourion-Arsiquaud S, Faibish D, Myers E, Spevak L, Compston J, Hodsman A, Shane E, Recker RR, Boskey ER, Boskey AL. Use of FTIR

spectroscopic imaging to identify parameters associated with fragility fracture. J Bone Miner Res. 2009;24:1565–71.

11. Yerramshetty JS, Akkus O. The associations between mineral crystallinity and the mechanical properties of human cortical bone. Bone. 2008;42:476–82.
12. Sasaki N, Sudoh Y. X-ray pole figure analysis of apatite crystals and collagen molecules in bone. Calcif Tissue Int. 1997;60:361–7.
13. Sasaki N, Matsushima N, Ikawa T, Yamamura H, Fukuda A. Orientation of bone mineral and its role in the anisotropic mechanical properties of bone—transverse anisotropy. J Biomech. 1989;22:157–64.
14. Bacon GE, Goodship AE. The orientation of the mineral crystals in the radius and tibia of the sheep, and its variation with age. J Anat. 1991;179:15–22.
15. Bacon GE, Griffiths RK. Texture, stress and age in the human femur. J Anat. 1985;143:97–101.
16. Wenk HR, Heidelbach F. Crystal alignment of carbonated apatite in bone and calcified tendon: results from quantitative texture analysis. Bone. 1999;24:361–9.
17. Gourion-Arsiquaud S, Allen MR, Burr DB, Vashishth D, Tang SY, Boskey AL. Bisphosphonate treatment modifies canine bone mineral and matrix properties and their heterogeneity. Bone. 2010;46:666–72.
18. Akkus O, Adar F, Schaffler MB. Age-related changes in physicochemical properties of mineral crystals are related to impaired mechanical function of cortical bone. Bone. 2004;34:443–53.
19. Boyde A, Riggs CM. The quantitative study of the orientation of collagen in compact bone slices. Bone. 1990;11:35–9.
20. Goldman HM, Bromage TG, Thomas CDL, Clement JG. Preferred collagen fiber orientation in the human mid-shaft femur. Anat Rec. 2003;272A:435–45.
21. Janko M, Davydovskaya P, Bauer M, Zink A, Stark RW. Anisotropic Raman scattering in collagen bundles. Opt Lett. 2010;35:2765–7.
22. Sasaki N, Ikawa T, Fukuda A. Orientation of mineral in bovine bone and the anisotropic mechanical properties of plexiform bone. J Biomech. 1991;24:57–61.
23. Martin RB, Boardman DL. The effects of collagen fiber orientation, porosity, density, and mineralization on bovine cortical bone bending properties. J Biomech. 1991;26:1047–54.
24. Martin RB, Ishida J. The relative effects of collagen fiber orientation, porosity, density and mineralisation on bone strength. J Biomech. 1989;22:419–26.
25. Liu Y, Manjubala I, Schell H, Epari DR, Roschger P, Duda GN, Fratzl P. Size and habit of mineral particles in bone and mineralized callus during bone healing in sheep. J Bone Miner Res. 2010;25:2029–38.
26. Cedola A, Mastrogiacomo M, Lagomarsino S, Cancedda R, Giannini C, Guagliardi A, Ladisa M, Burghammer M, Rustichelli F, Komlev V. Orientation of mineral crystals by collagen fibers during in vivo bone engineering: an X-ray diffraction imaging study. Spectrochim Acta B. 2007;62:642–7.
27. Cancedda R, Cedola A, Giuliani A, Komlev V, Lagomarsino S, Mastrogiacomo M, Peyrin F, Rustichelli F. Bulk and interface investigations of scaffolds and tissue-engineered bones by X-ray microtomography and X-ray microdiffraction. Biomaterials. 2007; 28:2505–24.
28. Nakano T, Kaibara K, Ishimoto T, Tabata Y, Umakoshi Y. Biological apatite (BAp) crystallographic orientation and texture as a new index for assessing the microstructure and function of bone regenerated by tissue engineering. Bone. 2012; 741–7.
29. Nakano T, Kaibara K, Tabata Y, Nagata N, Enomoto S, Marukawa E, Umakoshi Y. Analysis of hydroxyapatite (HAp) texture in regenerated hard tissues using micro-beam X-ray diffractometer technique. In: Ikada Y, Umakoshi Y, Hotta Y, eds. Tissue engineering for therapeutic use 6. Amsterdam: Elsevier Sciences; 2002. p. 95–104.
30. Ishimoto T, Nakano T, Umakoshi Y, Yamamoto M, Tabata Y. Role of stress distribution on healing process of preferential alignment of biological apatite in long bones. Mater Sci Forum. 2006;512:261–4.
31. Ishimoto T, Nakano T, Yamamoto M, Tabata Y. Biomechanical evaluation of regenerated long bone by nanoindentation. J Mater Sci Mater Med. 2011;22:969–76.
32. Hosseinkhani H, Hosseinkhani M, Khademhosseini A, Kobayashi H. Bone regeneration through controlled release of bone morphogenetic protein-2 from 3-D tissue engineered nano-scaffold. J Control Release. 2007;117:380–6.
33. Takahashi Y, Yamamoto M, Yamada K, Kawakami O, Tabata Y. Skull bone regeneration in nonhuman primates by controlled release of bone morphogenetic protein-2 from a biodegradable hydrogel. Tissue Eng. 2007;13:293–300.
34. Paris O. From diffraction to imaging: new avenues in studying hierarchical biological tissues with X-ray microbeams. Biointerphases. 2008;3:FB16–FB26.
35. Zegzula HD, Buck DC, Brekke J, Wozney JM, Hollinger JO. Bone formation with use of rhBMP-2 (recombinant human bone morphogenetic protein-2). J Bone Joint Surg. 1997;79A:1778–90.
36. Yamamoto M, Takahashi Y, Tabata Y. Enhanced bone regeneration at a segmental bone defect by controlled release of bone morphogenetic protein-2 from a biodegradable hydrogel. Tissue Eng. 2006; 12:1305–11.
37. Oliver WC, Pharr GM. An improved technique for determining hardness and elastic modulus using load and displacement sensing indentation experiments. J Mater Res. 1992;7:1564–83.
38. Yamamoto M, Takahashi Y, Tabata Y. Controlled release by biodegradable hydrogels enhances the ectopic bone formation of bone morphogenetic protein. Biomaterials. 2003;24:4375–83.
39. Yamaguchi A, Komori T, Suda T. Regulation of osteoblast differentiation mediated by bone morphogenetic proteins, hedgehogs, and Cbfa1. Endocr Rev. 2000;21:393–411.
40. Kadowaki A, Tsukazaki T, Hirata K, Shibata Y, Okubo Y, Bessho K, Komori T, Yoshida N, Yamaguchi A. Isolation and characterization of a mesenchymal cell line that differentiates into osteoblasts in response to BMP-2 from calvariae of GFP transgenic mice. Bone. 2004;34:993–1003.
41. Yamaguchi A, Katagiri T, Ikeda T, Wozney JM, Rosen V, Wang EA, Kahn AJ, Suda T, Yoshiki S. Recombinant human bone morphogenetic protein-2 stimulates osteoblastic maturation and inhibits myogenic differentiation in vitro. J Cell Biol. 1991;113:681–7.
42. Katagiri T, Yamaguchi A, Komai M, Abe E, Takahashi N, Ikeda T, Rosen V, Wozney JM, Fujisawa-Sehara A, Suda T. Bone morphogenetic protein-2 converts the differentiation pathway of C2C12 myoblasts into the osteoblast lineage. J Cell Biol. 1994;127:1755–66.
43. Yamagiwa H, Endo N, Tokunaga K, Hayami T, Hatano H, Takahashi HE. In vivo bone-forming capacity of human bone marrow-derived stromal cells is stimulated by recombinant human bone morphogenetic protein-2. J Bone Miner Metab. 2001;19:20–8.
44. Ishimoto T, Nakano T, Umakoshi Y, Yamamoto M, Tabata Y. Effects of applied stress on preferential alignment of biological apatite in rabbit forelimb bones. Phosph Res Bull. 2004;17:77–82.
45. Abe E, Yamamoto M, Taguchi Y, Lecka-Czernik B, O'Brien CA, Economides AN, Stahl N, Jilka RL, Manolagas SC. Essential requirement of BMP-2/4 for both osteoblast and osteoclast formation in murine bone marrow cultures from adult mice: antagonism by noggin. J Bone Miner Res. 2000;15:663–73.
46. Itoh K, Udagawa N, Katagiri T, Iemura S, Ueno N, Yasuda H, Higashio K, Quinn JMW, Gillespie MT, Martin TJ, Suda T, Takahashi N. Bone morphogenetic protein 2 stimulates osteoclast differentiation and survival supported by receptor activator of nuclear factor-kappaB ligand. Endocrinology. 2001;142:3656–62.

47. Kaneko H, Arakawa T, Mano H, Kaneda T, Ogasawara A, Nakagawa M, Toyama Y, Yabe Y, Kumegawa M, Hakeda Y. Direct stimulation of osteoclastic bone resorption by bone morphogenetic protein (BMP)-2 and expression of BMP receptors in mature osteoclast. Bone. 2000;27:479–86.
48. Li G, Bouxsein ML, Luppen C, Li XJ, Wood M, Seeherman HJ, Wozney JM, Simpson H. Bone consolidation is enhanced by hrBMP-2 in a rabbit model of distraction osteogenesis. J Orthop Res. 2002;20:779–88.
49. Morris MD, Mandair GS. Raman assessment of bone quality. Clin Orthop Relat Res. 2011;469:2160–9.
50. Ito M, Wakao N, Hida T, Matsui Y, Abe Y, Aoyagi K, Uetani M, Harada A. Analysis of hip geometry by clinical CT for the assessment of hip fracture risk in elderly Japanese women. Bone. 2010; 46:453–7.
51. Mashiba T, Mori S, Burr DB, Komatsubara S, Cao Y, Manabe T, Norimatsu H. The effects of suppressed bone remodeling by bisphosphonates on microdamage accumulation and degree of mineralization in the cortical bone of dog rib. J Bone Miner Metab. 2005;23:36–42.
52. Garnero P, Sornay-Rendu E, Claustrat B, Delmas PD. Biochemical markers of bone turnover, endogenous hormones and the risk of fractures in postmenopausal women: the OFELY study. J Bone Miner Res. 2000;15:1526–36.
53. Saito M, Marumo K. Collagen cross-links as a determinant of bone quality: a possible explanation for bone fragility in aging, osteoporosis, and diabetes mellitus. Osteoporos Int. 2010;21:195–214.
54. Shiraishi A, Miyabe S, Nakano T, Umakoshi Y, Ito M, Mihara M. The combination therapy with alfacalcidol and risedronate improves the mechanical property in lumbar spine by affecting the material properties in an ovariectomized rat model of osteoporosis. BMC Musculoskelet Disord. 2009;10:66.
55. Lee JW, Nakano T, Toyosawa S, Tabata Y, Umakoshi Y. Areal distribution of preferential alignment of biological apatite (BAp) crystallite on cross-section of center of femoral diaphysis in osteopetrotic (op/op) mouse. Mater Trans. 2007;48:337–42.